# ***Supporting Information***

# Highly Selective Reduction of $CO_2$ to $C_{2+}$ Hydrocarbons at Cu/Polyaniline Interfaces

Xing Wei[1], Zhenglei Yin[2], Kangjie Lyu[1], Zhen Li[1], Jun Gong[1], Gongwei Wang[1], Li Xiao[1,*], Juntao Lu[1], Lin Zhuang[1,2,*]

[1] *College of Chemistry and Molecular Sciences, Hubei Key Lab of Electrochemical Power Sources, Wuhan University, Wuhan 430072, China*

[2] *The Institute for Advanced Studies, Wuhan University, Wuhan 430072, China*

[*] Corresponding authors. E-mails: chem.lily@whu.edu.cn, lzhuang@whu.edu.cn

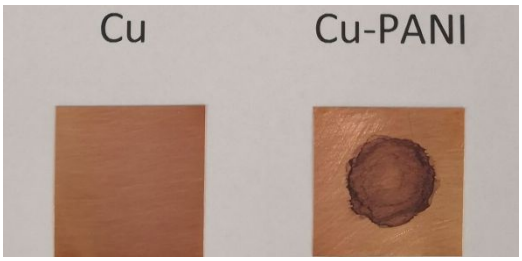


**Figure S1.** Photos of the as-prepared Cu and Cu-PANI electrodes.

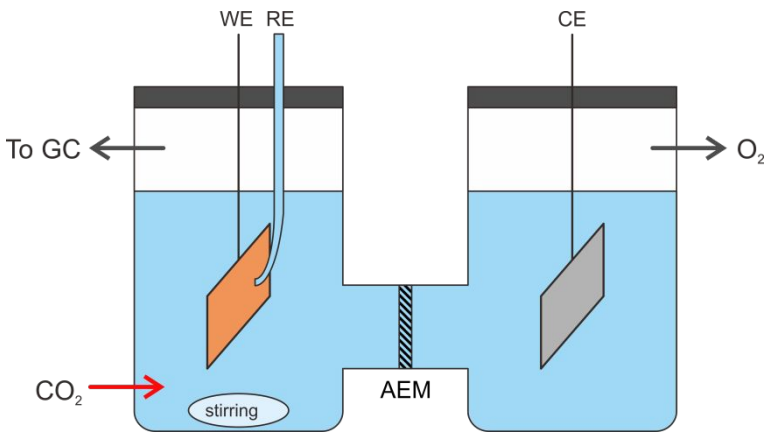


**Figure S2.** Schematic diagram of the H-type electrolytic cell.

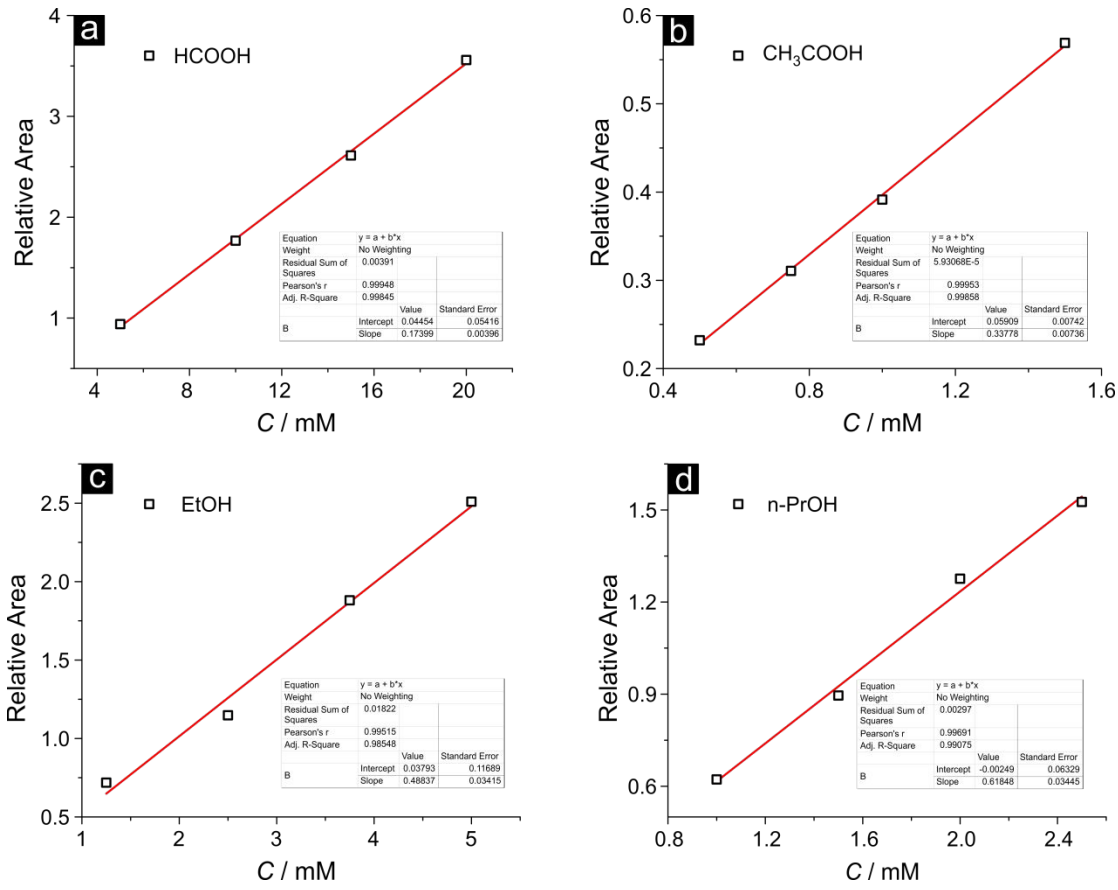


**Figure S3.** Standard curves of (a) HCOOH, (b) $CH_3COOH$, (c) EtOH, and (d) n-PrOH components for $^1H$ NMR quantitative analysis.

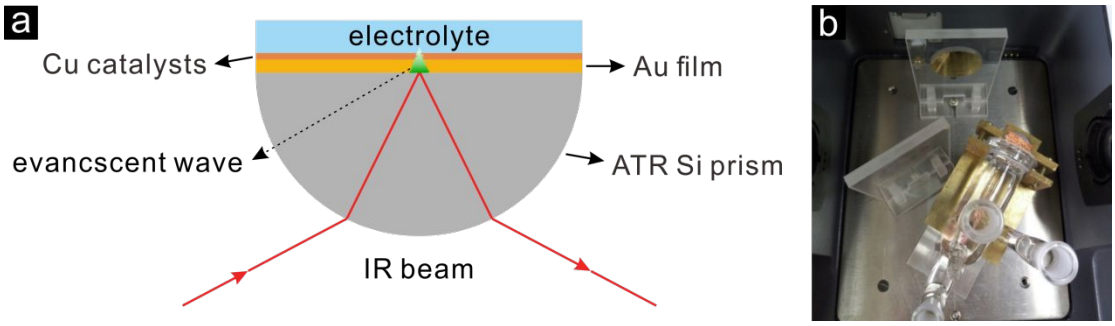


**Figure S4.** Experimental details for the ATR-SEIRAS measurements. (a) Schematic diagram of the attenuated total reflection (ATR) infrared spectroscopy and (b) the photo of the in-situ electrochemical cell placed inside the sample chamber of the FTIR instrument.

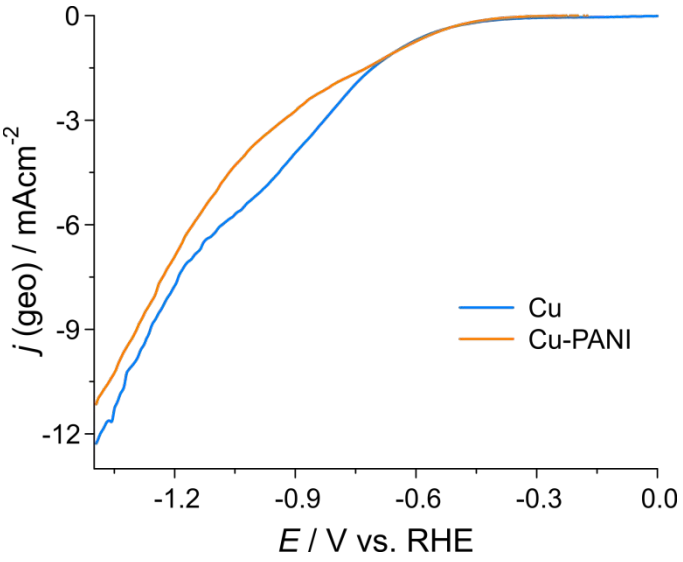


**Figure S5.** Electrochemical LSV curves of the Cu and Cu-PANI electrodes recorded during the ATR-SEIRAS experiment. The potential scan rate was 5 mV/s.

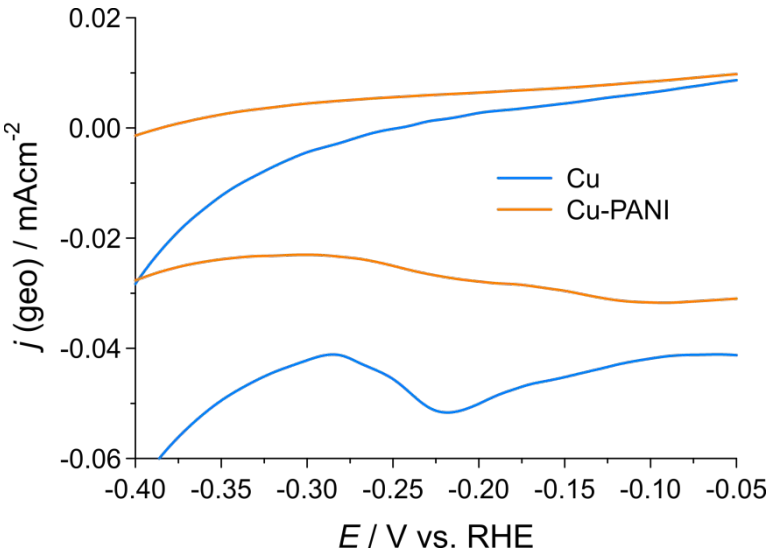


**Figure S6.** The enlarged view of the CV in Figure 1c. A weak reduction process corresponding the Cu+/Cu0 conversion can be observed at the potential region of 0.05 to -0.40 V. Scan rate = 100 mV/s.

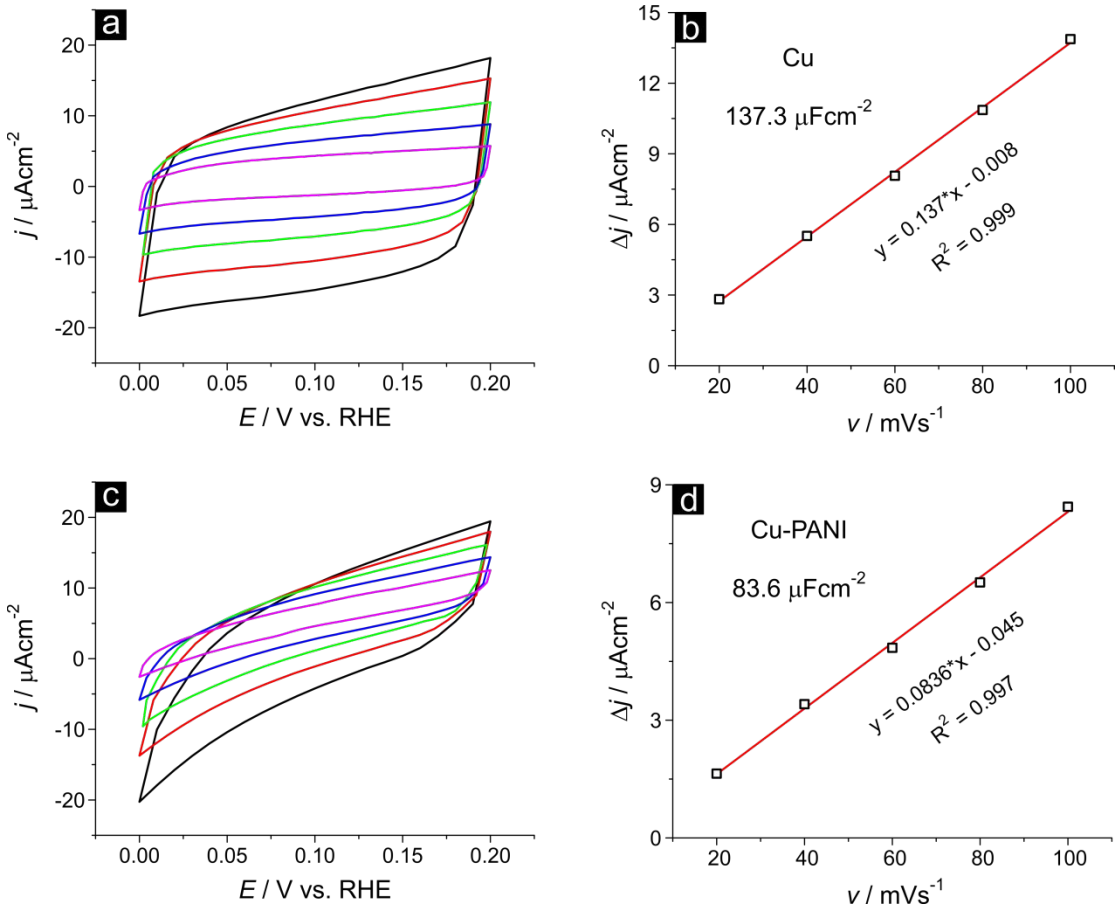


**Figure S7.** Cyclic voltammograms of (a) Cu foil and (c) Cu-PANI electrode in $N_2$ saturated 0.1 M $KHCO_3$ scanned from 0.2~0.4 V vs. RHE at various scan rates in order to estimate the double layer capacity; Current density plotted against CV scan rates for (b) Cu foil and (d) Cu-PANI electrode.

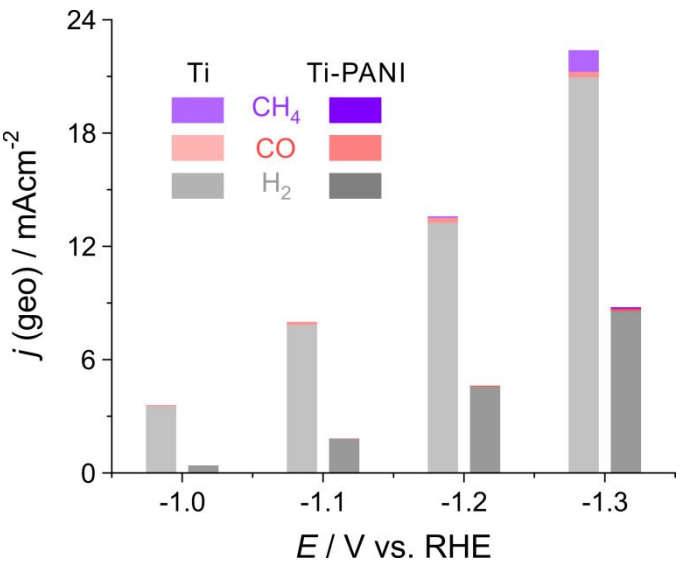


**Figure S8.** Electrochemical $CO_2$RR results on Ti and Ti-PANI electrodes.

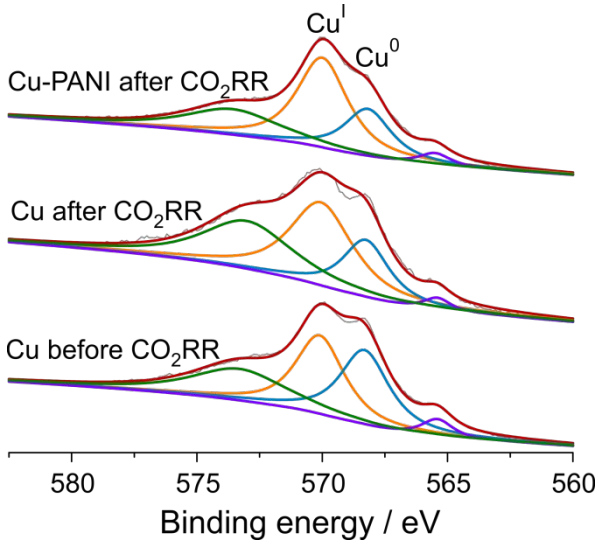


**Figure S9.** Cu LMM spectra of Cu electrode before and after $CO_2$RR, and the Cu-PANI electrode after $CO_2$RR with removal of PANI layer so as to test the underneath Cu.

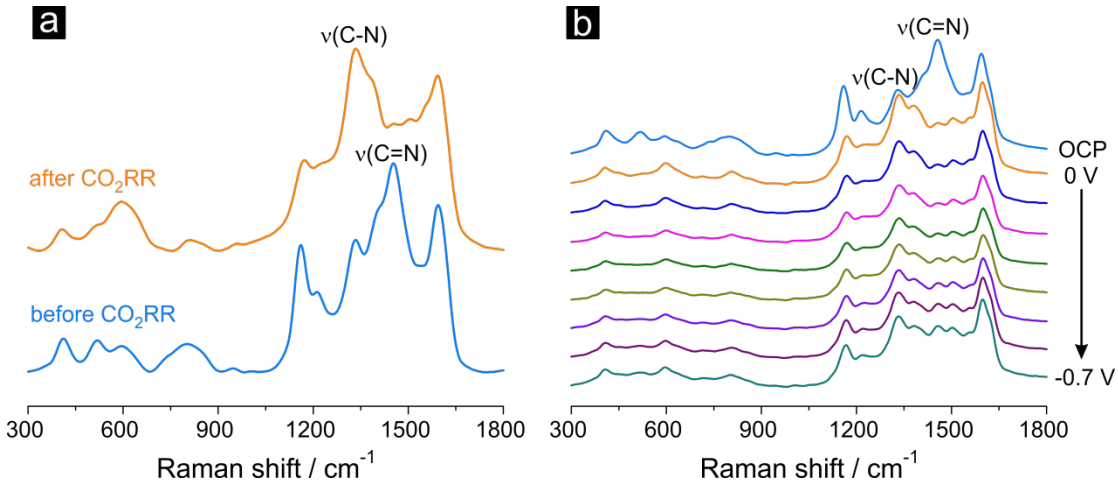


**Figure S10.** (a) Raman spectra of the Cu-PANI electrode before and after $CO_2$RR, and (b) *in situ* Raman spectra of PANI feature at the region of negative potentials.

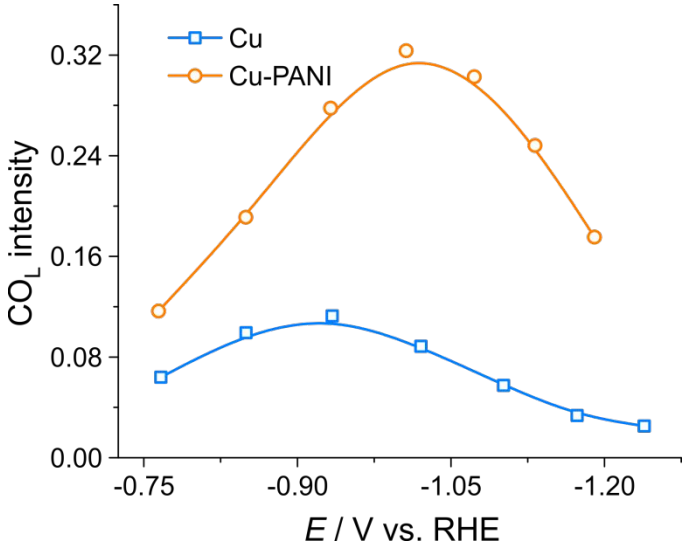


**Figure S11.** Potential-dependent FTIR signal intensity of $CO_L$ on Cu and Cu-PANI electrodes. All potentials were *iR* corrected.

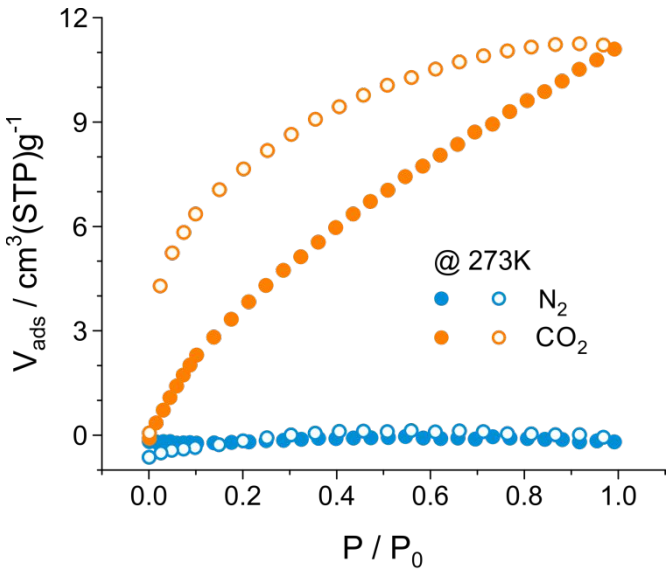


**Figure S12.** Gas adsorption isotherms of PANI powder for $N_2$ and $CO_2$ at 273K.

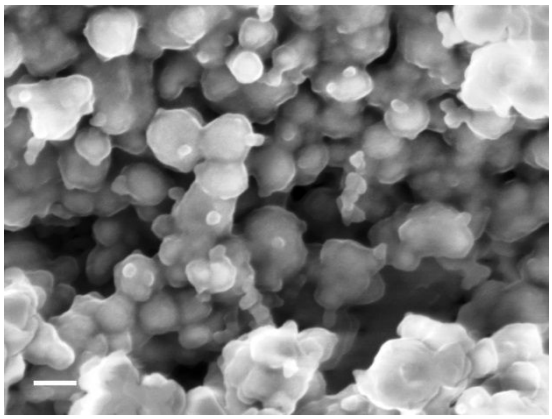

**Figure S13.** SEM image of as-prepared Cu-PANI nano-catalyst, scale bar = 100 nm.

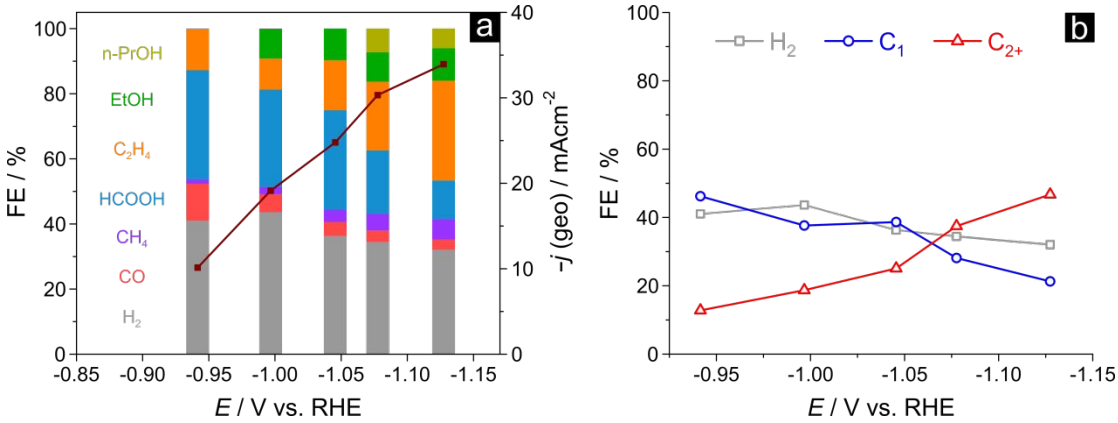


**Figure S14.** Electrochemical $CO_2RR$ performance of commercial Cu NPs. (a) The Faradaic efficiency of each product and total geometric current density and (b) The FE of $H_2$, $C_1$ and $C_{2+}$ production for the Cu/PANI catalyst.

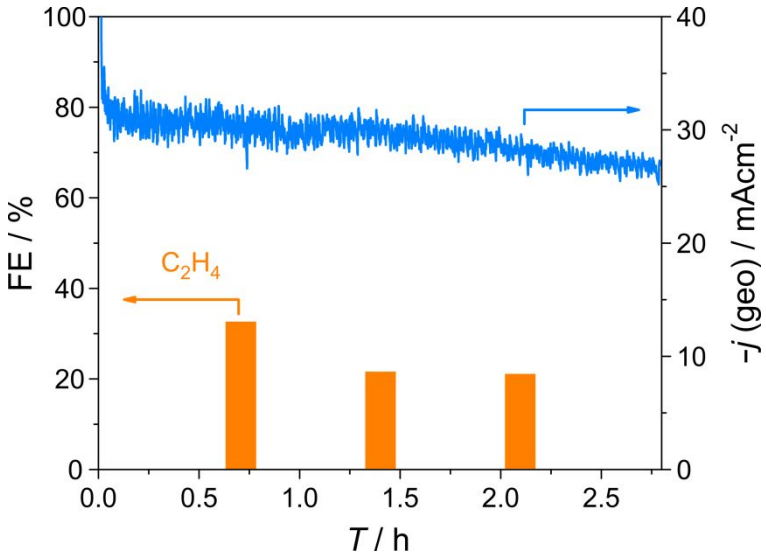


**Figure S15.** The stability in the FE of $C_2H_4$ and the current density of commercial Cu NPs at -1.08 $V_{RHE}$. The electrolyte was $CO_2$ saturated 0.1 M $KHCO_3$ solution, and the electrode potentials were *iR* corrected.

**Table S1.** Summary of electrochemical surface area and corresponding surface roughness factor for Cu and Cu-PANI electrodes. The geometric surface area for both Cu and Cu-PANI electrodes is 0.785cm$^2$. Taking polycrystalline Cu as the reference standard, the roughness factor is set to 1, and the double layer capacitance is 29 μF/cm$^2$.

| | **Cu foil** | **Cu-PANI** |
|---|---|---|
| Electrochemical Surface Area (ECSA) | 3.71 | 2.26 |
| Surface Roughness Factor (SRF) | 4.73 | 2.88 |

**Table S2.** Results of the Cu $2p_{3/2}$ peak fitting in Figure 3c.

| **Catalysts** | **Binding energy / eV** | | |
|---|---|---|---|
| | $Cu^0$ / $Cu^I$ | $Cu^{II}$ | $Cu^{II}$ satellite |
| Cu before $CO_2RR$ | 932.7 | 934.7 | 944.1 |
| Cu after $CO_2RR$ | 932.6 | 934.6 | 944.2 |
| Cu-PANI after $CO_2RR$ | 932.6 | 934.6 | 944.2 |

**Table S3.** Details of the Cu LMM peak fitting in Figure S6.

| Catalysts | Binding energy / eV | |
|---|---|---|
| | $Cu^0$ | $Cu^I$ |
| Cu before $CO_2RR$ | 568.3 | 570.1 |
| Cu after $CO_2RR$ | 568.3 | 570.1 |
| Cu-PANI after $CO_2RR$ | 568.2 | 570.0 |

**Table S4.** Comparison of Cu-based catalysts reported in the literature toward the $CO_2RR$ performance and stability in aqueous solution.

| Catalysts | Electrolyte | *j* (geo) / $mAcm^{-2}$ | *E* / V vs. RHE | $C_2H_4$ FE / % | $C_{2+}$ FE / % | Stability / h | Ref |
|---|---|---|---|---|---|---|---|
| Cu-PANI nano-catalyst | 0.1 M $KHCO_3$ | 28.3 | -1.08 | 43.8 | 77.4 | 20 | This work |
| Cu-PANI nano-catalyst | 0.1 M $KHCO_3$ | 34.7 | -1.13 | 48.8 | 78.4 | \ | This work |
| Amino acid modified Cu | 0.1 M $KHCO_3$ | 10.8 | -1.25 | 13 | 34.1 | 12 | 1 |
| Poly(acrylamide) modified Cu | 0.1 M $NaHCO_3$ | 60 | -0.96 | 26 | \ | 2 | 2 |
| Cu-porphyrin complex | 0.5 M $KHCO_3$ | 49 | -0.976 | 17 | \ | 1 | 3 |
| B-doped Cu | 0.1 M KCl | 70 | -1.1 | 52±2 | 79±2 | 40 | 4 |
| Hydrophobic Cu dendrites | 0.1 M $CsHCO_3$ | 30 | ~-1.4 | 56 | 74 | 5 | 5 |
| Bi-phasic $Cu_2O$-Cu | 0.1 M KCl | ~7 | -1.6 | 22 | 58.5 | 1 | 6 |
| Cu(100) single electrode | 0.1 M $KHCO_3$ | 5 | -1 | 40.4 | 57.8 | \ | 7 |
| Cu NPs covered Cu foil | 0.1 M $KClO_4$ | \ | -1.1 | 36 | \ | \ | 8 |
| Polycrystalline Cu | 0.1 M $KHCO_3$ | ~7.5 | -1.05 | 26 | 40.6 | 1 | 9 |
| 3 μm thick $Cu_2O$ | 0.5 M $NaHCO_3$ | 19.6 | -0.85 | 3.9 | 21.4 | \ | 10 |
| $Cu_2O$-derived Cu NPs | 0.1 M $KHCO_3$ | 38.5 | -1.1 | 32.5 | 34 | \ | 11 |
| $Cu_2O$ film on Cu disk | 0.1 M $KHCO_3$ | 34.4 | -0.99 | 37.5 | 54.8 | 1 | 12 |
| $O_2$ plasma Cu foil | 0.1 M $KHCO_3$ | 12 | -0.92 | 60 | \ | 5 | 13 |
| Oxide-derived Cu foam | 0.5 M $NaHCO_3$ | ~11.5 | -0.8 | 20 | 55 | \ | 14 |
| 44 nm Cu cubes | 0.1 M $KHCO_3$ | ~4 | -1.1 | 41.1 | 46.4 | 1 | 15 |
| Cu nanocubes | 0.25 M $KHCO_3$ | 68.1 | -0.96 | 32.5 | 60.5 | 2.5 | 16 |
| Anodized Cu nanowire arrays | 0.1 M $KHCO_3$ | 19.2 | -1.08 | 38.1 | ~60 | 40 | 17 |
| Electro-redeposition Cu | 0.1 M $KHCO_3$ | 57.9 | -1.2 | 38 | 54 | 1 | 18 |

"\" represents "not available".

**References**

(1) Xie, M. S.; Xia, B. Y.; Li, Y.; Yan, Y.; Yang, Y.; Sun, Q.; Chan, S. H.; Fisher, A.; Wang, X. Amino acid modified copper electrodes for the enhanced selective electroreduction of carbon dioxide towards hydrocarbons. *Energy Environ. Sci.* 2016, 9 (5), 1687−1695.

(2) Ahn, S.; Klyukin, K.; Wakeham, R. J.; Rudd, J. A.; Lewis, A. R.; Alexander, S.; Carla, F.; Alexandrov, V.; Andreoli, E. Poly-amide modified copper foam electrodes for enhanced electrochemical reduction of carbon dioxide. *ACS Catal.* 2018, 8 (5), 4132–4142.

(3) Weng, Z.; Jiang, J.; Wu, Y.; Wu, Z.; Guo, X.; Materna, K. L.; Liu, W.; Batista, V. S.; Brudvig, G. W.; Wang, H. Electrochemical $CO_2$ Reduction to Hydrocarbons on a Heterogeneous Molecular Cu Catalyst in Aqueous Solution. *J. Am. Chem. Soc.* 2016, 138 (26), 8076−8079.

(4) Zhou, Y.; Che, F.; Liu, M.; Zou, C.; Liang, Z.; De Luna, P.; Yuan, H.; Li, J.; Wang, Z.; Xie, H.; Li, H.; Chen, P.; Bladt, E.; Quintero-Bermudez, R.; Sham, T.-K.; Bals, S.; Hofkens, J.; Sinton, D.; Chen, G.; Sargent, E. H. Dopant-Induced Electron Localization Drives $CO_2$ Reduction to $C_2$ Hydrocarbons. *Nat. Chem.* 2018, 10 (9), 974−980.

(5) Wakerley, D.; Lamaison, S.; Ozanam, F.; Menguy, N.; Mercier, D.; Marcus, P.; Fontecave, M.; Mougel, V. Bio-inspired hydrophobicity promotes $CO_2$ reduction on a Cu surface. *Nat. Mater.* 2019, 1-6.

(6) Lee, S.; Kim, D.; Lee, J. Electrocatalytic production of C3-C4 compounds by conversion of $CO_2$ on a chloride-induced bi-phasic $Cu_2O$-Cu catalyst. *Angew. Chem. Int. Ed.* 2015, 127, 14914–14918.

(7) Hori, Y.; Takahashi, I.; Koga, O.; Hoshi, N. Electrochemical Reduction of Carbon Dioxide at Various Series of Copper Single Crystal Electrodes. *J. Mol. Catal. A: Chem.* 2003, 199 (1–2), 39−47.

(8) Tang, W.; Peterson, A. A.; Varela, A. S.; Jovanov, Z. P.; Bech, L.; Durand, W. J.; Dahl, S.; Norskov, J. K.; Chorkendorff, I. The Importance of Surface Morphology in Controlling the Selectivity of Polycrystalline Copper for CO2 Electroreduction. *Phys. Chem. Chem.Phys.* 2012, 14, 76−81.

(9) Kuhl, K. P.; Cave, E. R.; Abram, D. N.; Jaramillo, T. F. New Insights into the Electrochemical Reduction of Carbon Dioxide on Metallic Copper Surfaces. *Energy Environ.*

*Sci.* 2012, 5, 7050−7059.

(10) Li, C. W.; Kanan, M. W. $CO_2$ reduction at low overpotential on Cu electrodes resulting from the reduction of thick $Cu_2O$ films. *J. Am. Chem. Soc.* 2012, 134, 7231−7234.

(11) Kas, R.; Kortlever, R.; Milbrat, A.; Koper, M. T. M.; Mul, G.; Baltrusaitis, J. Electrochemical $CO_2$ reduction on $Cu_2O$-derived copper nanoparticles: controlling the catalytic selectivity of hydrocarbons. *Phys. Chem. Chem. Phys.* 2014, 16, 12194−201.

(12) Ren, D.; Deng, Y.; Handoko, A. D.; Chen, C. S.; Malkhandi, S.; Yeo, B. S. Selective Electrochemical Reduction of Carbon Dioxide to Ethylene and Ethanol on Copper(I) oxide catalysts. *ACS Catal.* 2015, 5, 2814−2821.

(13) Mistry, H.; Varela, A. S.; Bonifacio, C. S.; Zegkinoglou, I.; Sinev, I.; Choi, Y.-w.; Kisslinger, K.; Stach, E. A.; Yang, J. C.; Strasser, P.; Roldan Cuenya, B. Highly selective plasma-activated copper catalysts for carbon dioxide reduction to ethylene. *Nat. Commun.* 2016, 7, 12123.

(14) Dutta, A.; Rahaman, M.; Luedi, N. C.; Mohos, M.; Broekmann, P. Morphology Matters: Tuning the Product Distribution of $CO_2$ Electroreduction on Oxide-Derived Cu Foam Catalysts. *ACS Catal.* 2016, 6, 3804−3814.

(15) Loiudice, A.; Lobaccaro, P.; Kamali, E. A.; Thao, T.; Huang, B. H.; Ager, J. W.; Buonsanti, R. Tailoring Copper Nanocrystals towards $C_2$ Products in Electrochemical $CO_2$ Reduction. *Angew. Chem. Int. Ed.* 2016, 55, 5789−5792.

(16) Jiang, K.; Sandberg, R. B.; Akey, A. J.; Liu, X.; Bell, D.C.; Nørskov, J.K.; Chan, K.; Wang, H. Metal ion cycling of Cu foil for selective C–C coupling in electrochemical $CO_2$ reduction. *Nat. Catal.* 2018, 1 (2), 111−119.

(17) Lee, S. Y.; Jung, H.; Kim, N.-K.; Oh, H.-S.; Min, B. K.; Hwang, Y. J. Mixed Copper States in Anodized Cu Electrocatalyst for Stable and Selective Ethylene Production from $CO_2$ Reduction. *J. Am. Chem. Soc.* 2018, 140 (28), 8681–8689.

(18) De Luna, P.; Quintero-Bermudez, R.; Dinh, C.T.; Ross, M.B.; Bushuyev, O.S.; Todorović P.; Regier T.; Kelley, S.O.; Yang P.; Sargent E.H. Catalyst electro-redeposition controls morphology and oxidation state for selective carbon dioxide reduction. *Nat. Catal.* 2018, 1 (2), 103–110.